

ELECTRIC POTENTIAL AND TURBULENCE IN OH AND ECRH LOW-DENSITY PLASMAS IN THE T-10 TOKAMAK

A.V. MELNIKOV, L.G. ELISEEV, M.A. DRABINSKIY, S.A. GRASHIN, P.O. KHABANOV,
N.K. KHARCHEV, S.E. LYSENKO, V.N. ZENIN AND T-10 TEAM

National Research Centre 'Kurchatov Institute'

Moscow, Russia

Email: Melnikov_AV@nrcki.ru

M.V. UFIMTSEV

Moscow State University,

Moscow, Russia

Abstract

Geodesic Acoustic Modes (GAMs) and broadband ($f < 400$ kHz) turbulence of the plasma electrostatic potential and electron density have been directly studied in OH and ECRH plasmas in the T-10 tokamak. Potential and density fluctuations measurements were carried out with Heavy Ion Beam Probe (HIBP) from the plasma core to the edge. Four different types of modes were observed in T-10 plasmas: GAM ($f_{\text{GAM}}=20\text{-}25$ kHz) with higher frequency satellite ($f_{\text{sat}}=22\text{-}28$ kHz), Stochastic Low-Frequency Modes (SLF) with $f_{\text{SLF}}=0\text{-}30$ kHz, Low-Frequency Quasicoherent Modes (LFQC) with $f_{\text{LFQC}}=50\text{-}150$ kHz and High Frequency Quasi-Coherent modes (HFQC) with $f_{\text{HFQC}}=200\text{-}400$ kHz). Both GAM and satellite have homogeneous radial distribution of the frequency and amplitude of electric potential fluctuations in OH and ECRH plasmas. Cross-correlation analysis supports modes identification, while bicoherence analysis have shown three-wave interaction for both GAM and satellite.

1. INTRODUCTION

Plasma transport across magnetic field in magnetic traps, such as tokamaks and stellarators, is one of the critical issues of modern plasma physics. Plasma electrostatic potential ϕ (or radial electric field E_r) and its fluctuations are believed to play an important role in transport processes. It is expected that mean radial electric field E_r reduces turbulent transport across magnetic field lines due to turbulent eddies suppression by $E_r \times B_t$ shear. In addition, oscillatory component of E_r is linked to turbulence self-regulation mechanisms (zonal flows and geodesic-acoustic modes, GAM) [1, 2]. GAMs are now under the deep and extensive investigations in various fusion devices [3]. In T-10 tokamak GAMs are studied with correlation reflectometry (CR), Langmuir probes (LP) and heavy ion beam probe (HIBP) [4]. It has been shown recently, that electric potential oscillations associated with GAM have uniform poloidal structure ($m=0$) [5] and the features of the global plasma eigenmode [6]. Bispectral analysis has shown the nonlinear interaction between GAM and density broadband turbulence [7]. Recently three types of density fluctuations were observed in T-10 plasmas by CR: Stochastic Low-Frequency Modes (SLF, $f_{\text{SLF}}=0\text{-}30$ kHz [8]), Low Frequency Quasi-Coherent Modes (LFQC, $f_{\text{LFQC}}=50\text{-}150$ kHz [9]) and High Frequency Quasi-Coherent modes (HFQC, $f_{\text{HFQC}}=200\text{-}400$ kHz [10]). There are some indications on the role of these modes in plasma transport [9, 10], so the studies of the mode properties are of high importance. Previous studies with CR have described frequency regions and correlation properties of these modes [8, 9]. The present paper presents the new experimental observations on the plasma potential profiles and oscillations with a characterization of the mentioned modes with HIBP.

2. EXPERIMENTAL SET-UP

T-10 is a circular tokamak ($a = 0.3$ m, $R = 1.5$ m) with toroidal magnetic field $B_t = 1.5\text{-}2.4$ T and plasma current $I_p = 140\text{-}330$ kA. The plasma is limited by movable rail limiter at $a_{\text{lim}} = 0.27\text{-}0.3$ m, and a circular limiter at $a_{\text{clim}} = 0.33$ m. T-10 is equipped with HIBP diagnostics [11] which was recently upgraded to provide simultaneous measurements of the plasma electric potential and its fluctuations, and also the electron density and poloidal magnetic field fluctuations [12] from the plasma core to the edge (Fig. 1-a). To probe the plasma core at $B_t = 2.2$ T, Ti^+ ions with the energy of 330 keV are injected, and to probe the plasma edge, the energy is lowered to 200-180 keV. The 5-slit energy analyser (Fig. 1-b) allows simultaneous measurements at 5 observation points (sample volumes, SV) neighbouring in the plasma. Each SV has a length λ of about 1-2 cm with 0.5-1 cm poloidal distance between neighbouring SVs. Secondary ions from each of the five SVs go to 4 split-plate detector (Fig.1-c). The local plasma potential is proportional to the difference between primary and secondary beam energy:

$$\varphi^{SV} = \frac{E_a - E_b}{e} \sim \frac{i_1 + j_1 - i_2 - j_2}{i_1 + i_2 + j_1 + j_2},$$

where E_b is the energy of injected Tl^+ ions and E_d is the energy of detected Tl^{++} ions, which were ionized at the SV [13]. The energy of detected ions is proportional to vertical beam shift on the detector.

Secondary beam intensity $I_{tot} = i_1 + i_2 + j_1 + j_2$ (Fig.1-c) is proportional to local electron density multiplied by attenuation factors[13]:

$$I_{tot}(r_{SV}, t) = 2I_{inj}n(r_{SV})\sigma_{12}(r_{SV})\lambda(r_{SV})R_1R_2,$$

$$R_1 = \exp\left(-\int_{r_{inj}}^{r_{SV}} n(s)\sigma_{12}(s)ds\right), \quad R_2 = \exp\left(-\int_{r_{SV}}^{r_{det}} n(s)\sigma_{23}(s)ds\right),$$

where $n(r_{SV})$ is local electron density, σ_{12} and σ_{23} are the effective cross-sections for electron impact ionization of primary and secondary ions, λ is the length of the SV, R_1 and R_2 are the attenuation factors for primary and secondary trajectories (so-called ‘path integral effect’) [13]. For short-wave density fluctuations we can assume: $\delta I_{tot}(\rho, t)/I_{tot}(\rho) \approx \delta n_e(\rho, t)/n_e(\rho)$.

The poloidal magnetic field B_{pol} creates the Lorentz force, which leads to the appearance of a toroidal velocity component of the beam along the orbit:

$$m \frac{\partial \vec{V}}{\partial t} = Ze[\vec{V} \times \vec{B}].$$

Here V is the probing particle velocity, m is its mass and B is the total magnetic field. Thus, the poloidal field B_{pol} fluctuations may be retrieved from toroidal velocity V_ζ and shift ζ of the probing beam in the detector using the integral relations [13]:

$$\zeta \sim \frac{i_1 + i_2 - j_1 - j_2}{i_1 + i_2 + j_1 + j_2}.$$

During one shot, HIBP may operate in one of two modes: scanning mode, when the primary beam entrance angle into the plasma is periodically changed, and SV moves back and forth along the detector line, covering 3-5 cm of plasma radius, and the fixed-point mode, when the SV position is fixed during the plasma discharge. Scanning mode allows us to obtain the radial dependencies of plasma parameters over some radial interval, which can be changed with the probing beam energy. The fixed-point mode provides time-traces of measured plasma parameters n_e^{SV} , ϕ^{SV} and ζ , and gives extended time series for the cross-correlation analysis.

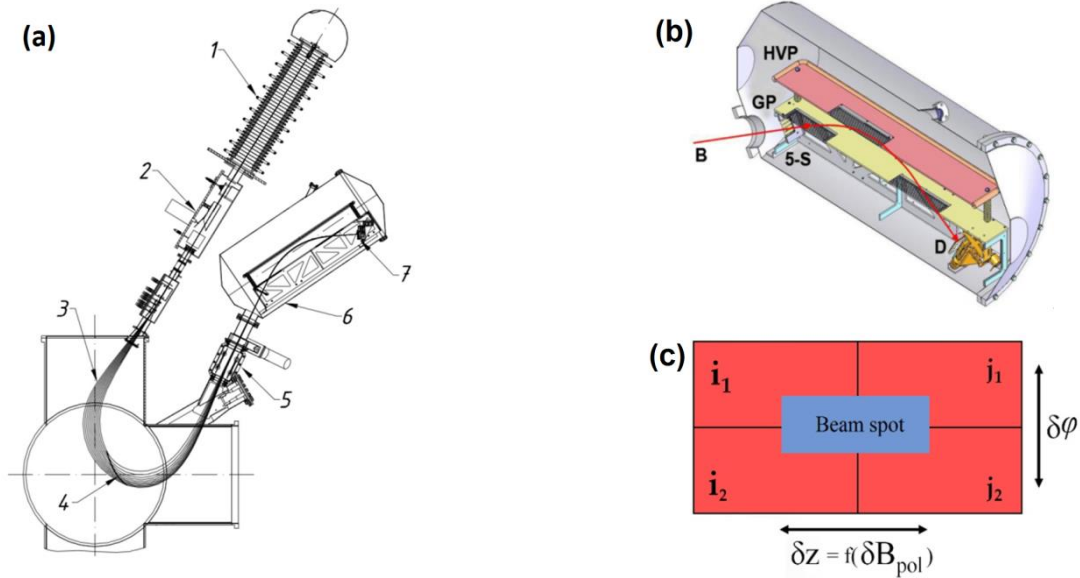


FIG. 1. a) HIBP on the T-10 tokamak: 1) beam injector, 2) primary beamline, 3) primary beam trajectories (Tl^+), 4) detector line, 5) secondary beam (Tl^{++}), 6) 5-slit energy analyser, 7) detector; b) 5-slit HIBP energy analyser: B is the secondary particle trajectory, 5-S is the entrance 5-slit assembly, GP is the ground plate, HVP is the high-voltage plate, G is grid, D is detector; c) HIBP detector schematic: i_1, i_2, j_1, j_2 are current to plates, $\delta\phi$ is signal of potential, δz is toroidal shift proportional to poloidal magnetic field.

3. EXPERIMENTAL RESULTS

3.1. Plasma electric potential

Radial profiles of electric potential ϕ were measured in T-10 OH plasmas with $B_t = 2.42$ T, $I_{pl} = 220$ kA by HIBP and Langmuir probe. In a series of reproducible discharges, the energy of Tl^+ beam changed from 210 keV to 265 keV to probe the plasma column from 28 cm to 20 cm, and the Langmuir probe scanned the plasma periphery from 31 to 28.5 cm. Figure 2 shows the obtained experimental data and linear fitting of HIBP data for $\bar{n}_e = 1 \times 10^{19} \text{ m}^{-3}$ (black) and $\bar{n}_e = 2 \times 10^{19} \text{ m}^{-3}$ (red). The HIBP plasma potential is in a good agreement with Langmuir probe data in terms of experimental errors. In the case of $\bar{n}_e = 1 \times 10^{19} \text{ m}^{-3}$ the plasma potential changes from $\phi = 100$ V at $r = 28$ cm to $\phi = -200$ V at $r = 20$ cm. With the rise of \bar{n}_e up to $2 \times 10^{19} \text{ m}^{-3}$ the electric potential values at the plasma periphery remain almost the same, while in the core plasma it becomes more negative: $\phi = -450$ V at $r = 20$ cm. Figure 2 shows that radially averaged electric field E_r is almost constant along the radius: $E_r = -33$ V/cm for $\bar{n}_e = 1 \times 10^{19} \text{ m}^{-3}$, while $E_r = -64$ V/cm for $\bar{n}_e = 2 \times 10^{19} \text{ m}^{-3}$. These results support the earlier data, measured for $B_t = 2.1$ T, $I_{pl} = 150$ kA [14, 15].

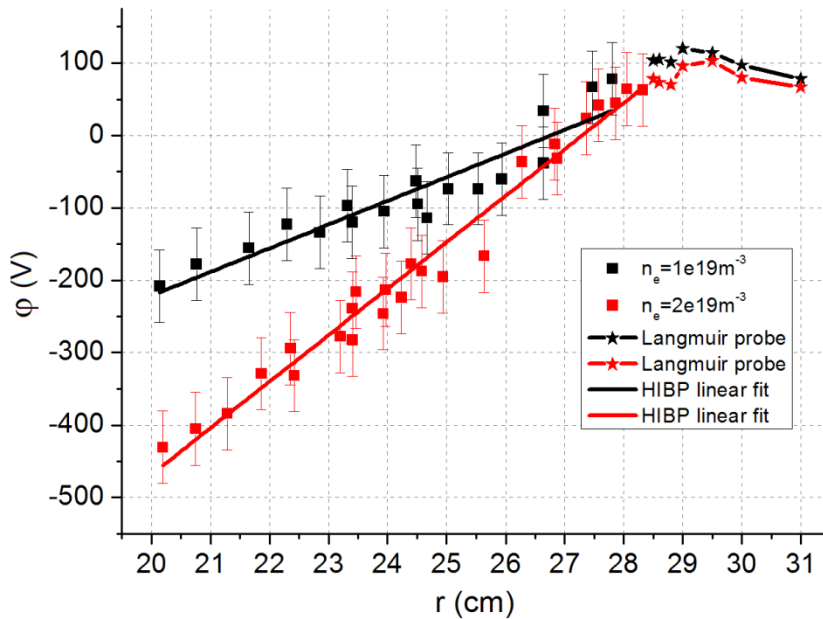


FIG. 2. Radial profile of plasma electric potential, measured with HIBP (squares) and Langmuir probe (stars). $B_t = 2.42$ T, $I_{pl} = 220$ kA, $\bar{n}_e = 1 \times 10^{19} \text{ m}^{-3}$ (black), $\bar{n}_e = 2 \times 10^{19} \text{ m}^{-3}$ (red).

3.2. Plasma turbulence

In the T-10 OH plasmas, four specific types of fluctuations are observed with HIBP in frequency range 0-450 kHz: geodesic acoustic modes (GAM), stochastic low-frequency (SLF), low frequency quasi-coherent (LFQC) and high-frequency quasi-coherent (HFQC). The detailed power spectra of HIBP potential and density signals for OH discharge with $B_t = 2.32$ T, $I_{pl} = 230$ kA and $\bar{n}_e = 2.3 \times 10^{19} \text{ m}^{-3}$ are presented in Fig. 3. All left figures show the whole frequency range under study from 0 to 450 kHz, the right ones – only low-frequency part of the spectra from 0 to 40 kHz. Figures 3-a and 3-b show the power spectra of HIBP total current I_{tot} and electric potential ϕ from the central (third) slit of the energy analyser, Figures 3-c and 3-d show the coherency and cross-phase respectively between plasma potentials from slits 2 and 3 (red lines) and those between I_{tot} from slits 2 and 3 (black lines). Poloidal distance $\Delta\lambda_{pol}$ between SV2 and SV3 related to slits 2 and 3 is around 1 cm. HIBP I_{tot} fluctuations represent the electron density fluctuations at the considered low-density plasmas. Figure 3 shows the presence of all four mentioned types of the modes: GAM and satellite in the PSDs and coherences, SLF in the PSDs and coherences, LFQC in the PSDs, coherences and phases. In contrast, HFQC is only visible in the density coherence and phase, but not in the PSDs and potential coherence and phase. It is worthwhile to note the evidence of the MHD-tearing mode with frequency ~ 7 rHz.

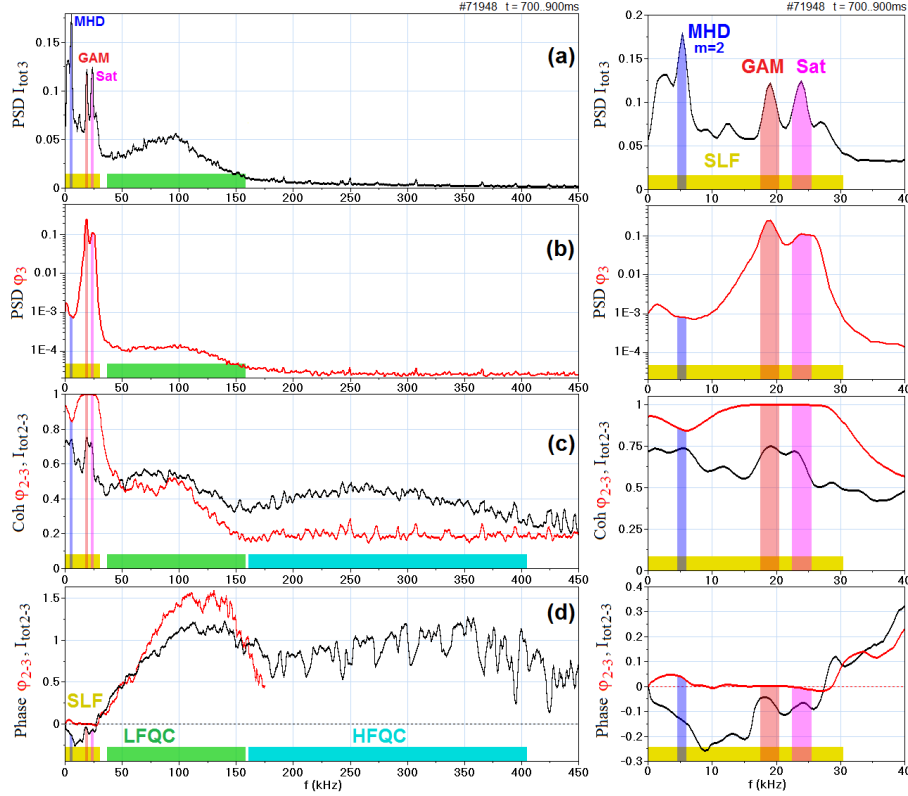


FIG. 3. #71948, $B_t = 2.32$ T, $I_{pl} = 230$ kA and $\bar{n}_e = 2.3 \times 10^{19} \text{ m}^{-3}$; power spectral density (PSD) of: a) HIBP I_{tot} ; b) plasma potential ϕ measured by HIBP, central slit #3, note the logarithmic scale; c) black line – coherency between potentials ϕ_2 and ϕ_3 , measured with slits 2 and 3, red line – coherency between HIBP I_{tot} measured with slits 2 and 3; d) black line – cross-phase between HIBP potentials ϕ_2 and ϕ_3 , measured with slits 2 and 3, red line – cross-phase between HIBP I_{tot} measured with slits 2 and 3.

3.2.1. Geodesic acoustic modes

In T-10 plasmas GAM is observed as monochromatic oscillations of electric potential at frequencies $f_{GAM} = 18\text{--}30$ kHz. An additional monochromatic satellite peak with frequencies $f_{SAT} = 20\text{--}35$ kHz is often accompanying the main GAM peak. In Fig. 3 strong GAM main and satellite peaks with $f_{GAM} = 18$ kHz and $f_{SAT} = 24$ kHz are clearly seen on power spectra of plasma potential (Fig.3-a) and electron density (Fig.3-b) oscillations. These peaks also show high level of coherency (Fig.3-c) and zero poloidal phase shift (Fig.3-d).

The radial profiles of GAM and satellite amplitudes were studied using HIBP in OH and ECRH plasmas with $B_t = 2.2$ T, $I_{pl} = 230$ kA and $\bar{n}_e = 1 \cdot 10^{19} \text{ m}^{-3}$. Three gyrotrons were used for ECRH scenario: one on-axis with $P_{ECRH-on} = 0.45$ MW and two off-axis with total power $P_{ECRH-off} = 1.7$ MW. Plasma scenario is shown on Fig. 4. All three gyrotrons switch on at $t \sim 700$ ms, and then at $t \sim 850$ ms off-axis gyrotrons switch off leaving only on-axis plasma heating. A series of reproducible shots was used to measure a radial profiles of plasma potential by radial interval of about 3-6 cm. The energy of the probing beam changed from 180 keV ($r_{SV} = 26\text{--}30$ cm) to 330 keV ($r_{SV} = 8\text{--}12$ cm) shot to shot [16]. Data was then combined to get radial distribution of power spectra of plasma potential perturbations, their amplitude and frequency radial dependencies (Fig. 5-6).

In the studied plasma scenario GAM at $f \sim 20\text{--}25$ kHz is observed with a satellite peak with $f \sim 25\text{--}30$ kHz. Fig. 5-a shows that in OH phase GAM and satellite both have a constant amplitude and frequency from the edge to the core of the plasma column. Potential perturbation for GAM and satellite peak are rather intensive with an amplitude close to 100 V. GAM amplitude decreases towards the edge starting at $r \sim 24$ cm, while amplitude of satellite starts to decrease at $r \sim 22$ cm. Application of the on-axis ECRH does not bring dramatic changes to the spatial structure of GAM and satellite, their frequencies remain almost the same, while the amplitude decreases to 85 V (Fig. 5-b). This may be explained by the density increase, which has been started during the combined ECRH phase and then further enhanced right after the switch-off of the on-axis ECRH up to $\bar{n}_e \sim 1.5 \cdot 10^{19} \text{ m}^{-3}$.

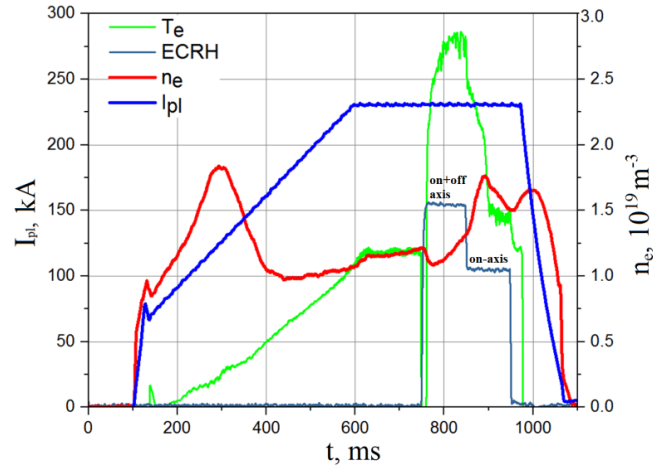


FIG. 4. Low-density T-10 shot scenario, #73198. $B_t = 2.2$ T, $I_{p1} = 230$ kA and $\bar{n}_e = 1 \times 10^{19} \text{ m}^{-3}$.

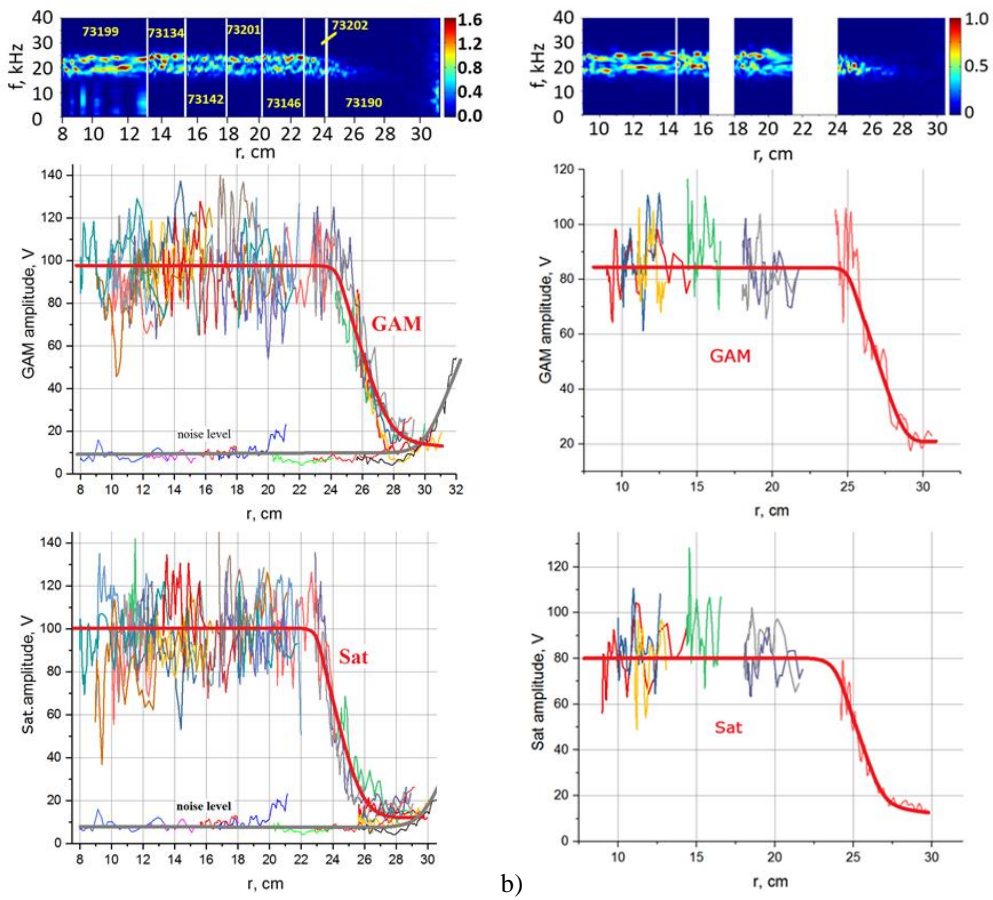


FIG. 5. Radial dependencies of power spectra and amplitude for GAM and satellite; a) OH; b) on-axis ECRH.

In contrast, during the combined on- and off-axis ECRH with high ECRH power, $P_{\text{ECRH}} = 2.2$ MW, the GAM features changed a lot – satellite disappears and GAM amplitude increases up to 260 V (Fig. 6). Both GAM and satellite demonstrate features of global modes with frequency and amplitude constant along the radius [6, 17]. Previous research has shown nonlinear interaction between GAM and broadband turbulence. High level of cross-bicoherence coefficient for the $(\varphi, I_{\text{tot}}, I_{\text{tot}})$ triad was found for GAM frequency in QC frequency range 50–150 kHz [7], indicating the three-wave interaction between GAM and turbulence. Bispectral analysis of new experimental data shows high level of cross-bicoherence coefficient for $(\varphi, I_{\text{tot}}, I_{\text{tot}})$ on both f_{GAM} and f_{SAT} for a wide frequency range up to 500 kHz (Fig. 7-a). Moreover, the statistically meaningful levels of bicoherence coefficient are now observed on QC frequencies for both GAM and satellite peaks (Fig. 7-a), which indicates

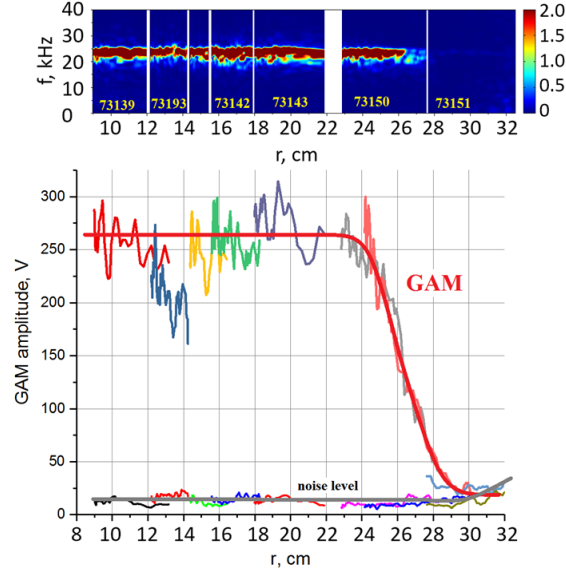


FIG.6. Radial dependencies of GAM power spectra and amplitude, ECRH on+off-axis.

that three wave interaction with broadband density turbulence takes place for both GAM main peak and satellite. In addition, cross-biphase (φ , I_{tot} , I_{tot}) has different sign for GAM and satellite in frequency ranges of LFQC 50-170 kHz. This indicates the differences in the character of the three-wave interaction between turbulence and GAM on the one hand, turbulence and satellite in another hand.

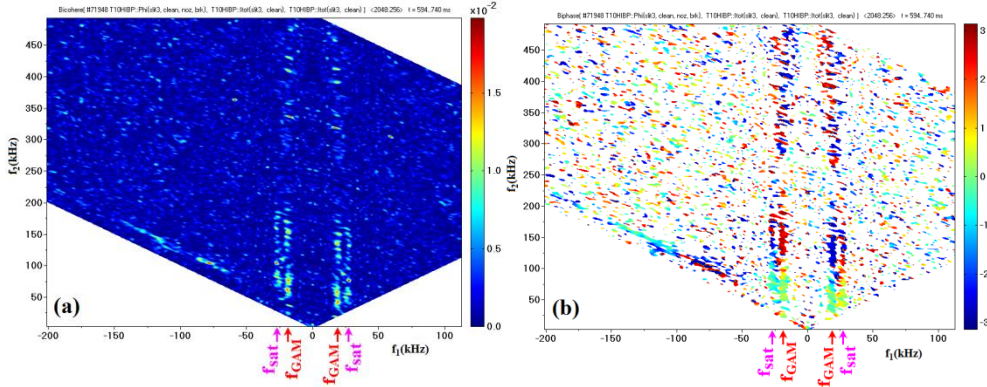


FIG. 7. #71948, $B_t = 2.32$ T, $I_{pl} = 230$ kA and $\bar{n}_e = 2.3 \times 10^{19} \text{ m}^{-3}$; a) bicoherence (φ , I , I); b) biphase (φ , I_{tot} , I_{tot}).

In top of that, for each GAM main peak and satellite, the sign of the cross-biphase (φ , I_{tot} , I_{tot}) in a low-frequency part of LFQC (50-100 kHz) is opposite to the one in a high-frequency part of LFQC (100 - 150 kHz) (Fig.7-b). Unless the cross-coherence coefficient for GAM frequency in HFQC frequency range 250-500 kHz is statistically meaningful, indicating the three-wave interaction between GAM and turbulence up to Nyquist frequency, the cross-biphase is not strictly determined in this high-frequency range.

3.2.2. Quasi-coherent modes

Low-Frequency Quasi-Coherent (LFQC) mode is observed as broad peak with $f_{\text{QC}} = 50\text{-}150$ kHz on density fluctuations both by CR and HIBP (Fig.3-a, Fig.8). Electrostatic potential component of QC is rather weak, four orders of magnitude smaller than GAM peak (Fig.3-b). Cross-correlation of potential signals from different slits is shown in Fig.8-a, while cross-correlation of the beam total currents I_{tot} is shown on Fig.8-b. As poloidal distance between SVs $\Delta\lambda_{\text{pol}}$ monotonically increases, taking value 1.1 cm (black curve), 2.8 cm (blue curve) and 4.9 cm (red curve) the coherence for both φ and I_{tot} monotonically decreases, which lets us to estimate the poloidal correlation length for LFQC as $\Delta\lambda_{\text{pol}}$ (LFQC) ~ 5 cm.

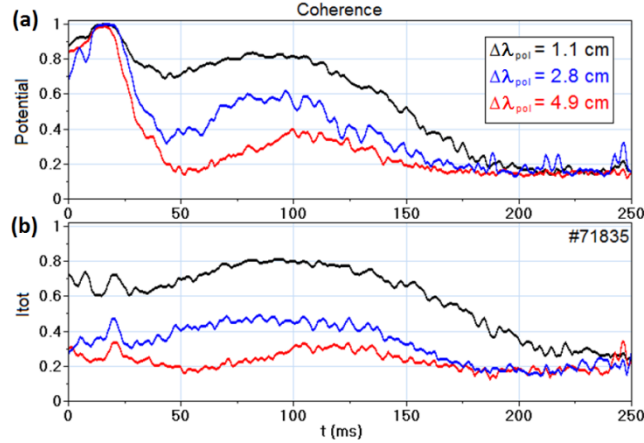


FIG. 8. Coherence between a) potentials ϕ and b) total currents I_{tot} from different poloidally shifted SVs.

High Frequency Quasi-Coherent mode (HFQC) is observed by CR in the frequency range $f_{HFQC} = 200-400$ kHz on density fluctuations. It is not seen on power spectra of HIBP I_{tot} but can be noticed on coherence between I_{tot} from different slits (Fig. 3-c).

3.2.3. Stochastic low-frequency modes

Stochastic low-frequency modes (SLF) were first observed in T-10 plasmas by CR in frequency range 0-30 kHz. Recent results show that SLF can also be detected with HIBP. Fig.3-a (right column) shows power spectra of HIBP I_{tot} , representing density fluctuations. The peak in frequency range below 5 kHz coincides with the area of high coherence (Fig.3-c) and negative phase shift (Fig.3-d) on density fluctuations. These distinctive features allow us to specify the observed fluctuations as SLF. In addition, negative phase shift on density fluctuations indicates the opposite direction of rotation, compared to LFQC with positive phase shift. Results obtained with CR confirm this feature of SLF [18]. The estimated poloidal correlation length for SLF is $\Delta\lambda_{pol}$ (SLF) ~ 3 cm.

4. DISCUSSIONS AND SUMMARY

Present experimental results on T-10 tokamak with HIBP confirm the earlier data. Electric potential profiles for plasma discharges with $B_t = 2.42$ T, $I_{pl} = 220$ kA measured with HIBP have almost linear shape and are in a good agreement with Langmuir probe data. Values of radial electric field are $E_r = -33$ V/cm for $\bar{n}_e = 1 \times 10^{19} \text{ m}^{-3}$ for and $E_r = -64$ V/cm for $\bar{n}_e = 2 \times 10^{19} \text{ m}^{-3}$.

Radial distribution of plasma potential in a wide radial range from $r = 8$ cm to $r = 30$ cm show that both GAM and satellite demonstrate the features of global eigenmodes with frequency and amplitude constant over the whole radial interval. On-axis ECRH regime is similar to OH in terms of GAM and satellite frequency and amplitude, while combined on- and off-axis ECRH leads to ~ 2 times increase of GAM amplitude. The raise in f_{GAM} is in agreement with the electron temperature increase due to ECRH. The satellite vanishing is an open question at the moment. Bispectral analysis shows high levels of bicoherence (ϕ, I_{tot}, I_{tot}) in QC frequency range not only for GAM but also for satellite. Biphasic (ϕ, I_{tot}, I_{tot}) for GAM and satellite have opposite sign in frequency ranges 50-100 kHz and 100-200 kHz.

Classification of fluctuation types observed with HIBP is confirmed by CR. Correlation analysis based on poloidally separated multi-point measurements shows high level of coherency of density fluctuations in frequency range 0-10 kHz, which is ascribed as SLF, and in frequency range 50-150 kHz, which is ascribed as LFQC. LFQC poloidal correlation length is estimated as ~ 5 cm. SLF fluctuations were described using HIBP data for the first time, its poloidal correlation length is estimated as ~ 1 cm. HFQC, which is pronounced in the density power spectra by CR is seen only on the coherence between I_{tot} signals from different slits. Additionally, SLF and LFQC density fluctuations show opposite poloidal phase shifts for $r < 20$ cm, indicating opposite poloidal rotation of these types of fluctuations, which is confirmed by CR experimental results. For $r > 20$ cm the poloidal phase shift for QC and SLF can have the same sign, indicating co-directional poloidal rotation. This preliminary observation needs further investigation.

ACKNOWLEDGEMENTS

The work was funded by Russian Science Foundation (project 14-22-00193) and in part by Rosatom contract No. 1/15470-D/230/1040-18. A.V. Melnikov was partly supported by the Competitiveness Program of NRNU MEPhI.

REFERENCES

- [1] DIAMOND P.H. et al., Zonal flows in plasma—a review, *Plasma Phys. Control. Fusion* **47** (2005) R35-R161.
- [2] WINSOR N. et al., Geodesic acoustic waves in hydromagnetic systems, *Phys. Fluids* **11** (1968) 2448-2450.
- [3] FUJISAWA A. et al., Experimental progress on zonal flow physics in toroidal plasmas, *Nucl. Fusion* **47** (2007) S718-S726.
- [4] MELNIKOV A.V. et al., Investigation of geodesic acoustic mode oscillations in the T-10 tokamak, *Plasma Phys. Control. Fusion* **48** (2006) S87-S110.
- [5] ZENIN V.N. et al., Study of poloidal structure of geodesic acoustic modes in the T-10 tokamak with heavy ion beam probing, *Probl. At. Sci. Technol. Ser. Plasma Phys.* **94** (2014) 269-271.
- [6] MELNIKOV A.V. et al., The features of the global GAM in OH and ECRH plasmas in the T-10 tokamak, *Nucl. Fusion* **55** (2015) 063001.
- [7] MELNIKOV A.V. et al., Study of interactions between GAMs and broadband turbulence in the T-10 tokamak, *Nucl. Fusion* **57** (2017) 115001.
- [8] VERSHKOV V.A. et al., Summary of experimental core turbulence characteristics in ohmic and electron cyclotron resonance heated discharges in T-10 tokamak plasmas, *Nucl. Fusion* **45** (2005) S203-S226.
- [9] VERSHKOV V.A. et al., Review of recent experiments on the T-10 tokamak with all metal wall, *Nucl. Fusion* **57** (2017) 102017.
- [10] VERSHKOV V.A. et al., Density fluctuations as an intrinsic mechanism of pressure profile formation, *Nucl. Fusion* **55** (2015) 063014.
- [11] MELNIKOV A.V. et al., HIBP diagnostics on T-10, *Rev. Sci. Instrum.* **66** (1995) 317.
- [12] MELNIKOV A.V. et al., Heavy ion beam probing—diagnostics to study potential and turbulence in toroidal plasmas, *Nucl. Fusion* **57** (2017) 072004.
- [13] DNESTROVSKIY Y.N. et al., Development of heavy ion beam probe diagnostics, *IEEE Trans. Plasma Sci.* **22** (1994) 310.
- [14] MELNIKOV A.V. et al., Electric potential dynamics in OH and ECRH plasmas in the T-10 tokamak, *Nucl. Fusion* **53** (2013) 093019.
- [15] MELNIKOV A.V. et al., ECRH effect on the electric potential and turbulence in the TJ-II stellarator and T-10 tokamak plasmas, *Plasma Phys. Control. Fusion* **60** (2018) 084008.
- [16] MELNIKOV A.V. et al., GAM and Broadband Turbulence Structure in OH and ECRH Plasmas in the T-10 Tokamak, *Plasma and Fusion Research*, **13** (2018) 3402109
- [17] MELNIKOV A.V. et al., Radial homogeneity of geodesic acoustic modes in ohmic discharges with low B in the T-10 tokamak, *Jetp Lett.* (2015) 100: 555
- [18] VERSHKOV V.A. et al., 3D structure of density fluctuations in T-10 tokamak and new approach for current profile estimation, *IAEA 27-th Fusion Energy Conf. 2018. EX/10-2.*